The Use of Eddy Current Sensor for Harmonic Force Prediction

Bor-Tsuen Wang[1], Shu-Hsin Lu [2]

[1] Professor [2] Graduate student
Department of Mechanical Engineering
National Pingtung University of Science and Technology
Pingtung, 91207
TAIWAN

Nomenclatures

A_b	the cross sectional area of beam
b_b	beam width
C_b	damping coefficient of beam
E_b	Young's Modulus of beam
$F(x,t)$	force function acting on beam
F_j	the *j*-th impact force amplitude
f_n	the *n*-th natural frequency of beam
f_s	harmonic excitation frequency
I_b	cross sectional moment of inertia of the beam
L_b	beam length
N	number of modes
N_t	number of time data points
Q_t	objective function
$q_n(t)$	modal coordinate
t_b	beam thickness
$w(x,t)$	beam lateral displacement
$w(x_i,t)=w_i(t)$	predicted displacement response of beam
$\hat{w}(x_i,t)=\hat{w}_i(t)$	measured displacement response of beam
W	beam displacement amplitude
x_j	the location of the *j*-th harmonic force in *x*-coordinate
x_i	the location of the *i*-th accelerometer sensor in *x*-coordinate
$\omega_s=2\pi f_s$	excitation frequency
$\omega_n=2\pi f_n$	the *n*-th natural frequency of beam
ρ_b	beam density
ξ_n	the *n*-th modal damping ratio of beam
$\phi_n(x)$	the *n*-th displacement mode shape of beam
$\phi_{n,j}=\phi_n(x_j)$	the *n*-th hammer mode shape function of beam at the *j*-th location of the hammer actuator

ABSTRACT

This paper presents the application of Eddy current sensor (ECS) as the sensing device to force prediction problem for cantilever beam structure. First, both the theoretical and experimental modal analyses are performed to obtain modal parameters of the beam, including natural frequencies, damping ratios and mode shapes. As the unknown harmonic force acting on the beam, the displacement response can then be measured by ECS and recorded. Since the exerted harmonic force is assumed as the ideal point force in spatial coordinate, the beam displacement response can be predicted and expressed as functions of the amplitude and location of the unknown harmonic force. The optimization problem is then constructed by defining the objective function as the mean square errors between the predicted and measured displacement response. With the resolution of the optimization problem, design variables, i.e. the amplitude and location of the unknown harmonic force, can be determined, simultaneously. Results show that the ECS is successfully applied to predict the unknown harmonic force contents. In the future, ECS can also be applied to force prediction problems for other structures such as rotor system.

Keywords: force prediction, harmonic force, cantilever beam, optimization

I. Introduction

Harmonic force prediction is an important issue in engineering applications. For example, rotating machineries are often operated in constant speed and result in harmonic response. The source of harmonic excitation can be incurred from imbalance force effect due to inhomogeneous material or assembly tolerance. The occurrence of the harmonic forces in rotating systems is expected but difficult to quantify their amplitudes and locations directly. Thus, the prediction of harmonic forces through indirect methods has drawn much attention. Verhoeven [1] developed an indirect method to identify hydraulic excitation force for centrifugal pumps and hydraulic turbines. The inversion of transfer function matrices must be obtained and can be critical to prediction accuracy. Besides, the restriction is that the number of response measurement locations must be the same as the number of forces to be determined. Karlsson [2] formulated an indirect harmonic force measurement technique. By measuring harmonic vibration of a linear structure, he presented an inverse process to predict the unknown complex amplitudes of harmonic forces with the known spatial distribution. D'Cruz et al. [3] numerically predicted the location, amplitude and phase of the harmonic force acting on a plate.

Wang [4] categorized the force prediction models into two types: direct method and optimization method. The drawback of direct method is that the force location must be known in priori. The optimization method is a general approach to solve for the force contents. However, the difficulty in solving the optimization problem is that many design variables related to the force contents can be involved. This paper will modify Wang's formulation [4] and reduce the number of design variables for one location index only.

For the prediction of unknown forces acting on structure, the selection of sensors to monitor the system response is required. Different types of sensors have been adopted to develop the force prediction model, such as strain gauges [5,6], accelerometers [7-9], laser vibrometer [10] and piezoelectric sensors [11]. Eddy current sensor (ECS) has been widely used in industrial applications. In particular, proximity measurement using ECS is one of frequently adopted methods to detect the displacement response of the target. Sadler and Ahn [12] applied ECS to detect small cracks in both aluminum and titanium. Wilde and Lai [13] optimally designed an ECS to detect vibrations in rotating turbine blades. The finite element model containing coil, turbine blade and air was constructed to perform harmonic electromagnetic simulation. The optimal mounting position of a sensor was found to measure the movement of turbine. Yamaguchi et al. [14] developed a method for directly measuring bearing wear by ECS. The fixed the ECS on the bearing stand to measure decreases in metal size due to bearing wear. In this work, the ECS is adopted to measure the beam displacement response due to harmonic force excitation.

This paper slightly modifies Wang's method [4] and follows its formulation to develop the prediction model for unknown harmonic force. Section II details the beam response analysis and the development of harmonic prediction model. Sections III and IV describe the implementation of prediction program and the experimental work, respectively. Section V shows both the theoretical and experimental prediction results, respectively, and demonstrates the feasibility of the developed force prediction model.

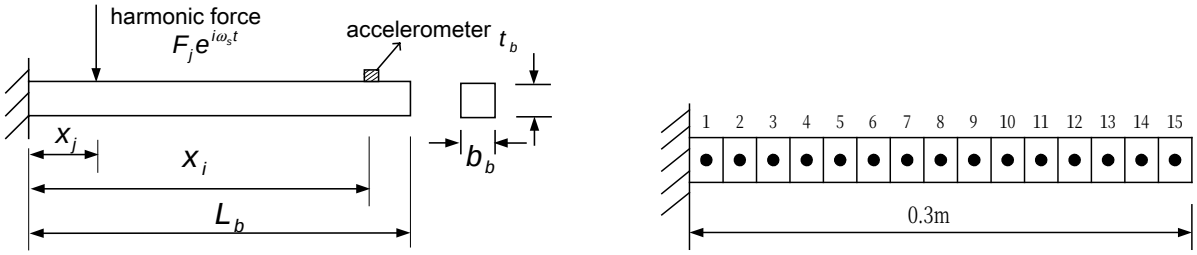

(a) system diagram **(b) test grid points**

Figure 1. Cantilever beam system diagram

II. Theoretical Analysis:

2.1 Beam Response analysis

Consider a uniform cantilever beam as shown in Figure 1(a). The system equation of motion for lateral vibration analysis can be written [15]:

$$E_b I_b \frac{\partial^4 w(x,t)}{\partial x^4} + C_b \frac{\partial w(x,t)}{\partial t} + \rho_b A_b \frac{\partial^2 w(x,t)}{\partial t^2} = F(x,t) \tag{1}$$

If the applied force is harmonic acting at $x = x_j$, the force function can be expressed:

$$F(x,t) = F_j \delta(x - x_j) e^{i\omega_s t} \tag{2}$$

where Delta function $\delta(x - x_j)$ represents the harmonic force location. From expansion theorem, the beam response can be assumed:

$$w(x,t) = \sum_{n=1}^{\infty} \phi_n(x) q_n(t) = \sum_{n=1}^{\infty} \phi_n(x) Q_n e^{i\omega_s t} \tag{3}$$

By the substitution of Equation (3) into Equation (1), the beam displacement at $x = x_i$ can be derived:

$$w(x_i,t) = \sum_{n=1}^{\infty} \phi_n(x_i) Q_n e^{i\omega_s t} = e^{i\omega_s t} \sum_{k=1}^{\infty} \frac{F_j \phi_n(x_j) \phi_n(x_i)}{(\omega_n^2 - \omega_s^2) + i(2\xi_n \omega_n \omega_s)} = W e^{i\omega_s t} \tag{4}$$

where

$$W = \sum_{n=1}^{\infty} \frac{F_j \phi_n(x_j) \phi_n(x_i)}{(\omega_n^2 - \omega_s^2) + i(2\xi_n \omega_n \omega_s)} \tag{5}$$

One can observe that beam displacement is functions of modal parameters, i.e. ω_n, ξ_n and ϕ_n, as well as the harmonic force amplitude F_j, excitation frequency $\omega_s = 2\pi f_s$ and its location x_j.It is noted that in numerical simulation only *N* modes are included to calculate the beam displacement.

2.2 Development of Harmonic Force Prediction Model

The conceptual diagram for force prediction model is depicted in Figure 2. For a structure subjected to unknown force, the ECS can detect the structural response as the input to the prediction model. Once the system modal parameters are also known, the force contents, including force amplitude and its location can be determined. This work deals with the prediction of unknown harmonic force acting on the cantilever beam. The ECS is employed to measure the beam response as the input to the prediction model. The system modal parameters, including natural frequencies, damping ratios and mode shapes, that can be determined theoretically or experimentally are also assumed known. The force prediction model will be developed to determine the force amplitude and its location, simultaneously. The optimization problem to predict the unknown harmonic force is formulated as follows:

Objective function:

$$Q_t = \sum_{r=1}^{N_t} [w_i(t_r) - \hat{w}_i(t_r)]^2 = \sum_{r=1}^{N_t} \left[\sum_{n=1}^{\infty} \frac{F_j \phi_n(x_j) \phi_n(x_i)}{(\omega_n^2 - \omega_s^2) + i(2\xi_n \omega_n \omega_s)} e^{i\omega_s t_r} - \hat{w}_i(t_r) \right]^2 \tag{6}$$

Design variables:

$$F_j, j \tag{7}$$

When $j = 1$, $\phi_n(x_j)$ equal to $\phi_n(x_1), n = 1,2,...,N$, and etc. The objective function Q_t is defined as the sum of

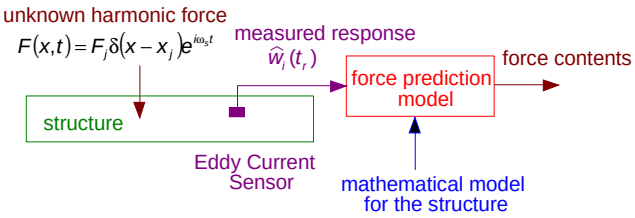

Figure 2. Conceptual diagram for force prediction

Table 1. Beam dimensions and material properties

Material	Steel
Length (L_b)	0.3 m
Width (b_b)	0.04 m
Thickness (t_b)	0.0016 m
Density (ρ_b)	7870 kg/m^3
Young's Modulus (E_b)	199×10^9 N/m^2
Poisson ratio (υ_b)	0.292

Table 2. Natural frequencies and damping ratios of cantilever beam

Mode	Experimental (Hz)	Theoretical (Hz)	Error (%)	Damping ratio (%)
1	14.02	14.44	2.91	1.29
2	90.14	90.49	0.39	0.29
3	253.00	253.39	0.15	0.09
4	497.24	496.57	-0.13	0.07

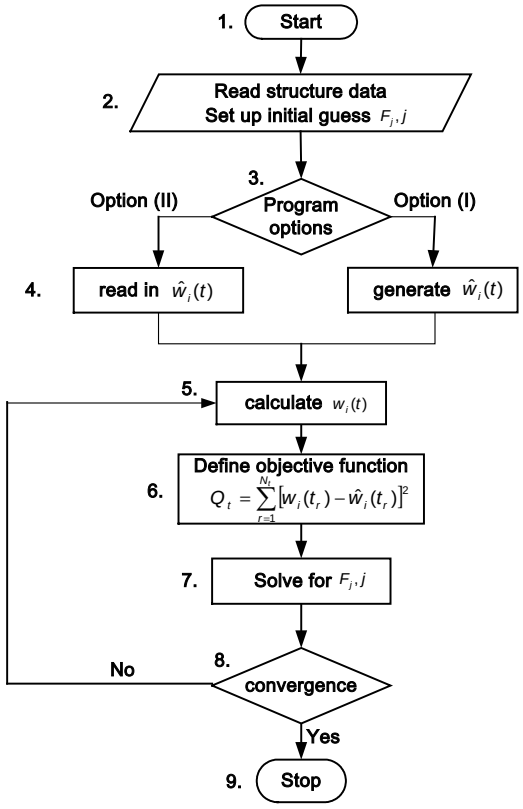

Figure 3. Force prediction program flowchart

square errors between the measured displacement $\hat{w}_i(t_r)$ and the predicted displacement $w_i(t_r)$ over the time range from t_1 to t_{N_t}. As shown in Equation (4), the predicted displacement $w_i(t_r)$ is functions of structural modal parameters and force contents. Structural modal parameters can be known. The unknown force contents are the force amplitude F_j and its location x_j, while the force excitation frequency ω_s can be easily detected. The design variables can then be identified as F_j and j. The index j related to the location x_j will result in $\phi_n(x_j), n=1,2,...,N$. By the resolution of the optimization problem, the unknown harmonic force amplitude and its location index j can be determined simultaneously. The objective of the optimization problem is, therefore, to find F_j and j so as to minimize the sum of square errors between $\hat{w}_i(t_r)$ and $w_i(t_r)$.

III. Development of Prediction Program

The force prediction program is implemented with Compaq Visual FORTRAN [16]. The IMSL optimization subroutine DBCPOL [17], which adopts direct search complex algorithm to solve general optimization problem with multiple design variables, is used to solve for the design variables, i.e. the force amplitude F_j and its location index j. The force prediction program flow chart is shown in Figure 3. There are two program options. Option (I) uses theoretically determined modal parameters and the specified harmonic force to generate the theoretical beam displacement response to represent the measured response $\hat{w}_i(t_r)$ for the verification of the force prediction model. Option (II) deals with the experimental validation. Program will read in experimentally measured beam displacement $\hat{w}_i(t_r)$ to predict the unknown applied harmonic force contents. Both theoretical and experimental prediction results will be presented in Section V.

IV. Experimental Setup

Table 1 shows the beam dimensions and its material properties. Conventional modal testing is carried out to obtain the beam modal parameters and validated with theoretical modal analysis [18]. The test grid points on the beam

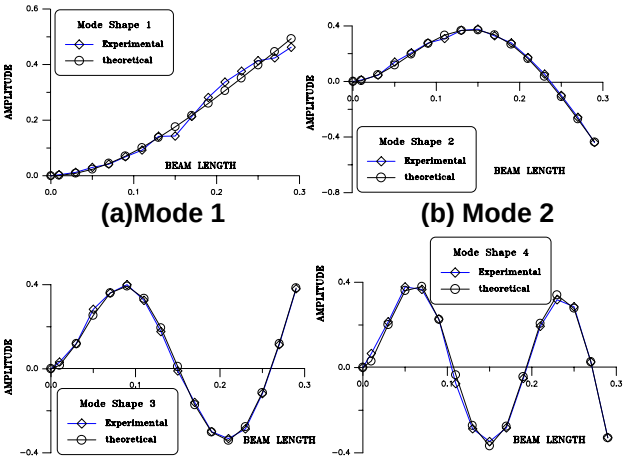

Figure 4. mode shapes of cantilever beam

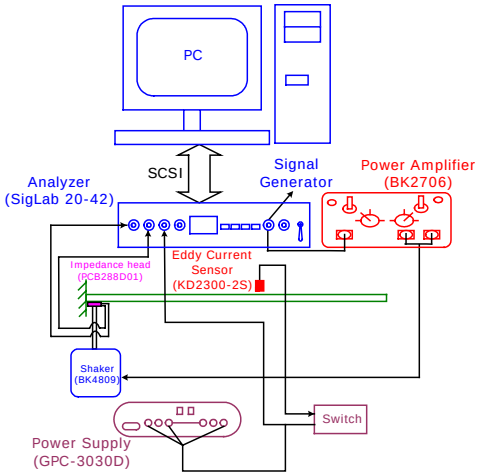

Figure 5. Experimental setup for harmonic force prediction

are shown in Figure 1(b). The first four natural frequencies of bending modes and the corresponding damping ratios are listed in Table 2. The first four bending mode shapes are shown in Figure 4. As one can observe the modal parameters agree well between theoretical and experimental analysis.

Figure 5 shows the experimental layout for harmonic force prediction. The mini shaker (BK4809) is used to simulate the harmonic force. The built-in signal generator of the analyzer (SigLab 20-42) can control different force levels and excitation frequencies. The eddy current sensor (KD2300-2S) is applied to measure the beam response $\hat{w}_i(t_r)$ due to the harmonic force excitation. The harmonic force amplitude F_j can be monitored through the impedance head (PCB288D01) connected to the analyzer. The force prediction program is operated off-line to determine the force amplitude F_j and location index j with the input of $\hat{w}_i(t_r)$ and the determined structural modal parameters.

V. Results and Discussions

5.1 Theoretical prediction results – Option (I)

This section presents the harmonic force prediction results by option (I), i.e. the theoretical approach to verify the feasibility of the developed force prediction model. The following conditions are studied: (1) different force locations, (2) different force amplitudes, (3) different excitation frequencies and (4) different sensor locations.

Figures 6 and 7 show the prediction results for different force locations for on-resonance and off-resonance excitation, respectively. The legend (2,3) shown in Figure 6 denotes (i,j)=(2,3), i.e. the force applied at position j=3, and the sensor at location i=2. Figure 6(a) and (b) are the prediction historical trends for both force amplitude and location, when the excitation frequency is $f_s = 14.02\text{Hz} \approx f_1$ near the first natural frequency. As one can see both force amplitude and location converge to the exact solution. The prediction historical trend varies largely in the initial stage of iteration and finally converges to exact solution. Figure 7 reveals the similar results except that the excitation frequency is $f_1 < f_s = 50\text{Hz} < f_2$, i.e. between the first and second resonant frequencies. From Figure 6 and 7, one can see the prediction algorithm works very well and predicts the force amplitudes and their locations correctly.

In order to further study the effect of force amplitudes on the prediction model, different force amplitudes are applied. Figure 8 and 9 show the prediction results for both on-resonance ($f_s = 14.02\text{Hz} \approx f_1$) and off-resonance ($f_1 < f_s = 50\text{Hz} < f_2$) excitation cases, respectively. Exact predictions of force amplitudes and locations can be achieved.

Figure 10 shows the prediction results for the first ($f_s = 14.02\text{Hz} \approx f_1$) and second ($f_s = 90.14\text{Hz} \approx f_2$) mode resonant excitation cases, and Figure 11 is for off-resonance excitation f_s=30, 50, 70 and 80 Hz. The optimal solutions converge to the exact value of force amplitude and location index correctly.

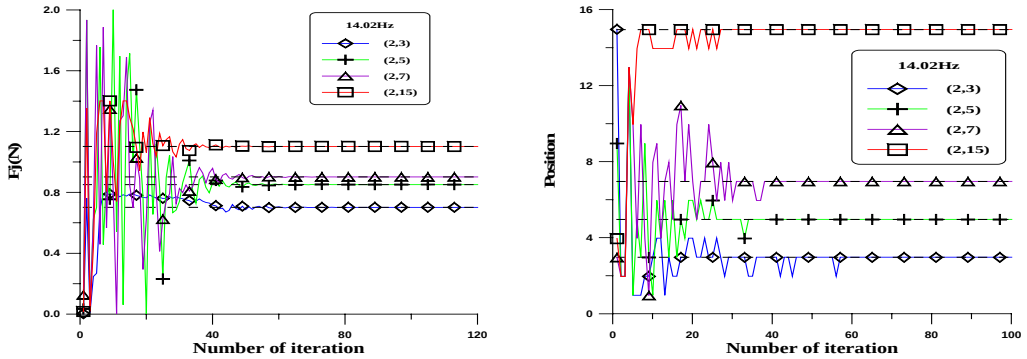

(a) force amplitude (b) force location

Figure 6. Option (I): prediction results for different force locations, $f_s = 14.02\text{Hz} \approx f_1$

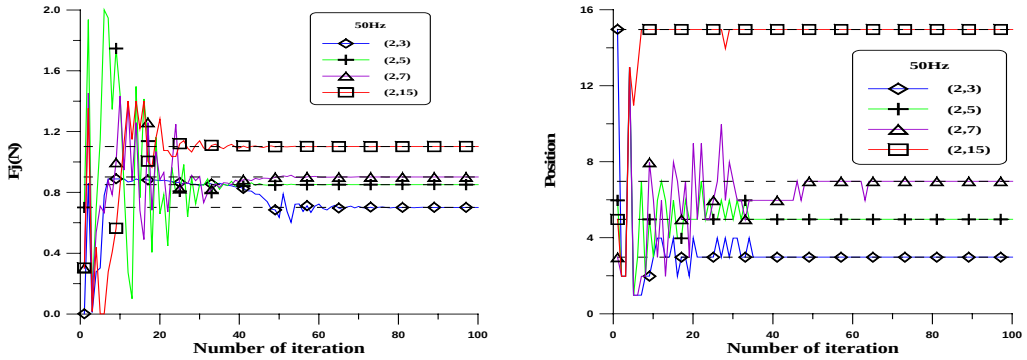

(a) force amplitude (b) force location

Figure 7. Option (I): prediction results for different force locations, $f_1 < f_s = 50\text{Hz} < f_2$

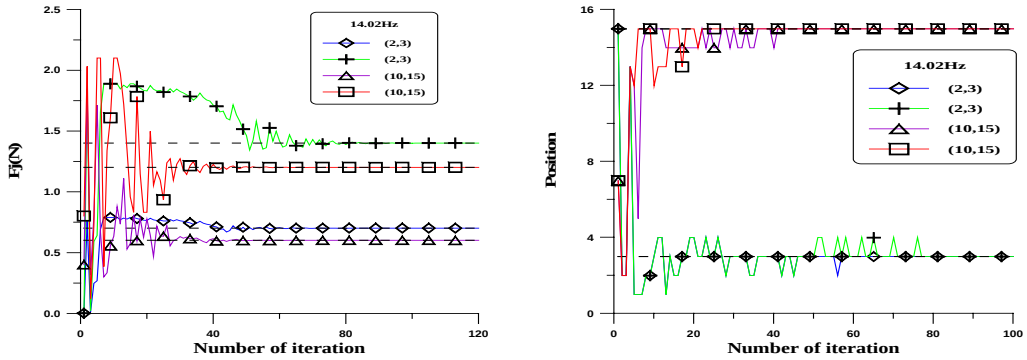

(a) force amplitude (b) force location

Figure 8. Option (I): prediction results for different force amplitudes, $f_s = 14.02\text{Hz} \approx f_1$

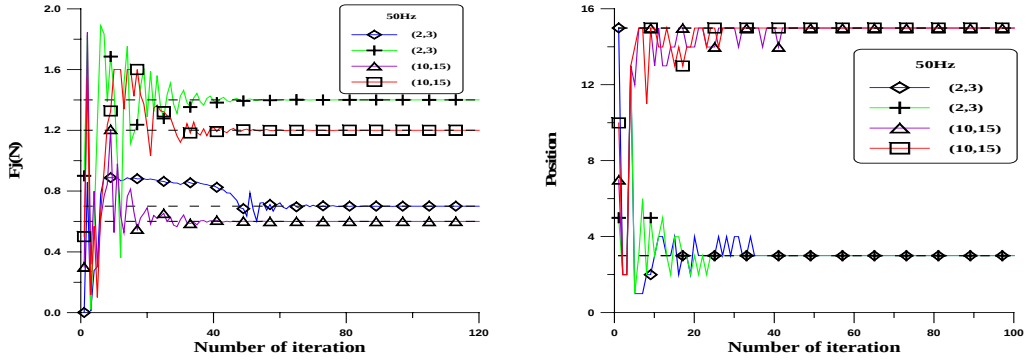

(a) force amplitude (b) force location

Figure 9. Option (I): prediction results for different force amplitudes, $f_1 < f_s = 50\text{Hz} < f_2$

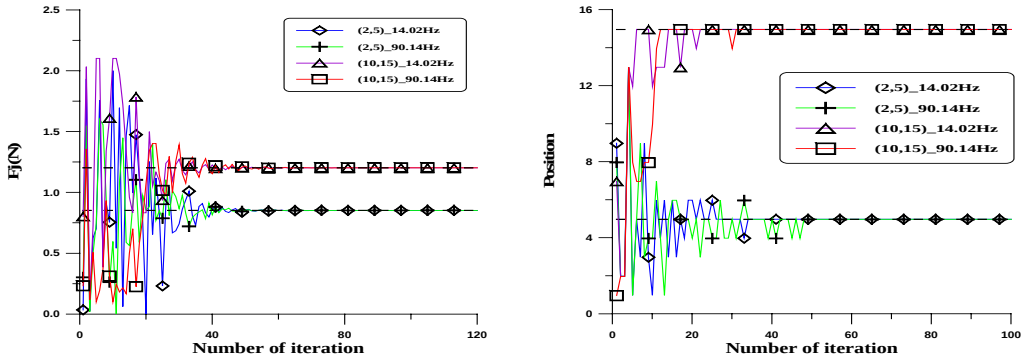

(a) force amplitude (b) force location

Figure 10. Option (I): prediction results for different excitation frequencies (on-resonance excitation)

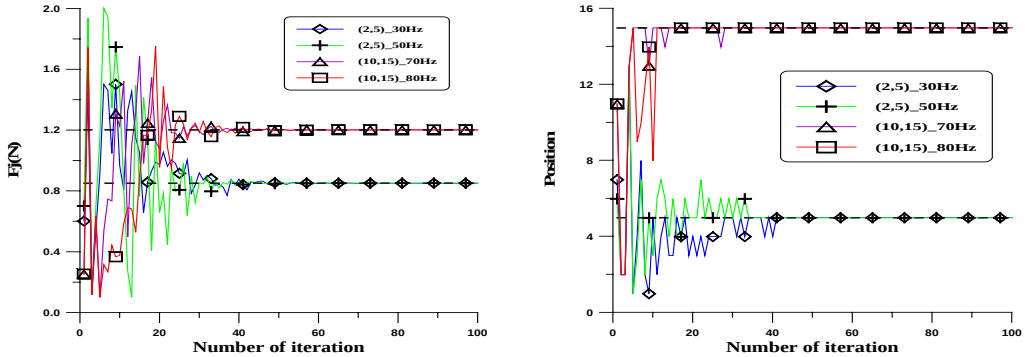

(a) force amplitude (b) force location

Figure 11. Option (I): prediction results for different excitation frequencies (off-resonance excitation)

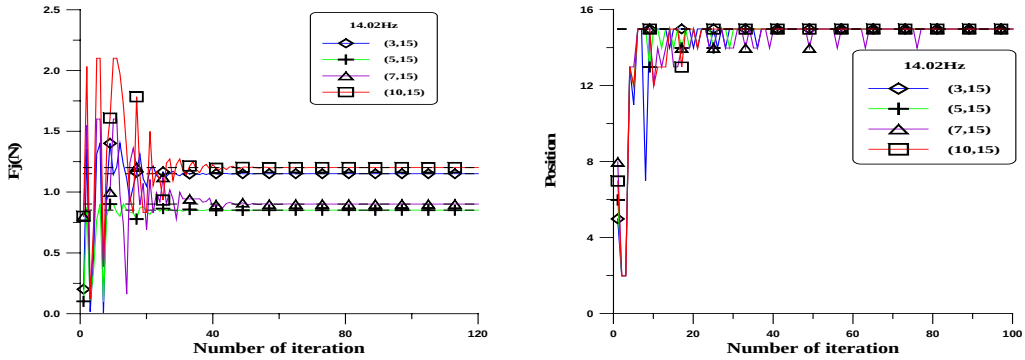

(a) force amplitude (b) force location

Figure 12. Option (I): prediction results for different sensor locations, $f_s = 14.02\text{Hz} \approx f_1$

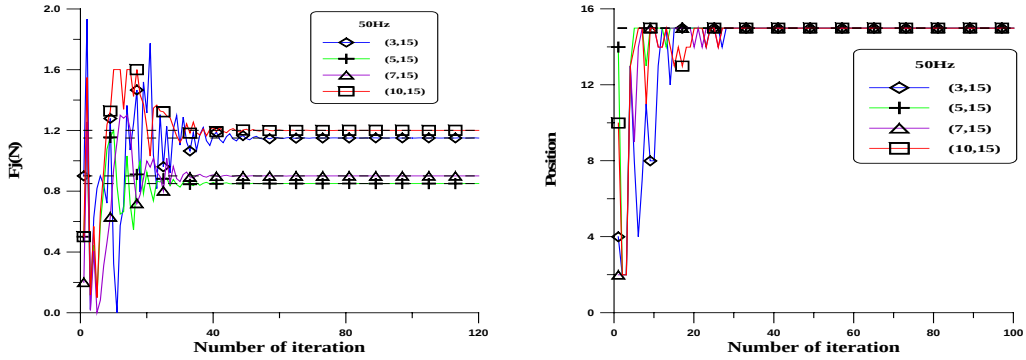

(a) force amplitude (b) force location

Figure 13. Option (I): prediction results for different force amplitudes, $f_1 < f_s = 50\text{Hz} < f_2$

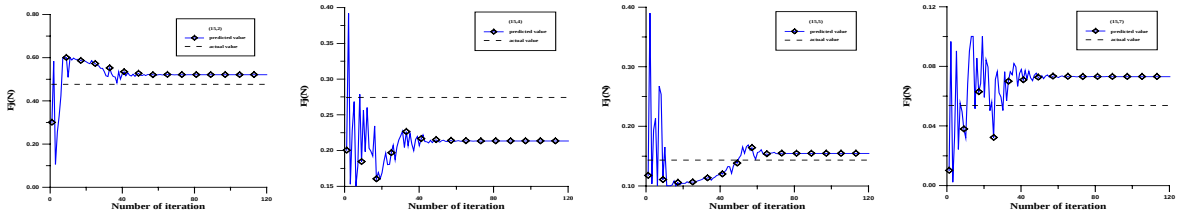

(a) (15,2), F_j =0.476N (b) (15,4), F_j =0.274N (c) (15,5), F_j =0.143N (d) (15,7), F_j =0.0536N

Figure 14. Option (II): force amplitude prediction convergence lines, $f_s = 14.02\text{Hz} \approx f_1$

Finally, it is also interested to know whether the sensor location will affect the prediction results. Figure 12(a) and (b) show the prediction historical trends of force amplitude and location index, respectively, for the first mode excitation, while Figure 13 is for the off-resonant excitation case, $f_1 < f_s = 50\text{Hz} < f_2$. The solutions also converge very well.

In summary, according to the above discussions base on Option (I) approach the force prediction model is feasible and also works well for different force amplitudes, locations, excitation frequencies and sensor location. Next, the experimental approach by Option (II) will be discussed.

5.2 Experimental prediction results – Option (II)

The experimental setup is as described in Section III. The harmonic force is emulated by a shaker and applied at the designated location. The force amplitude can be measured for comparison. The ECS is also located as prescribed to measure the beam displacement due to the harmonic excitation. The recorded displacement response is as the input to the prediction program. For the present work, the off-line force prediction is applied.

Table 3 shows the prediction results for different force locations for on-resonance excitation $f_s = 14.02\text{Hz} \approx f_1$. The prediction errors of amplitudes are within 10% for two cases. For the case of (*i*,*j*)=(15,4), the error is about –22% due to the incorrect prediction of force location. The bad prediction for the case of (*i*,*j*)=(15,7) is due to the low force amplitude. The amplitude converge line is shown in Figure 14 and reveals that the optimization solver works and converges optimal values. The location prediction is correct except the case of (*i*,*j*)=(15,4). Figure 15 shows the prediction historical trends of force location.

Table 4 shows prediction results for different force amplitudes for $f_s = 14.02\text{Hz} \approx f_1$. The force locations are correctly predicted, while the force amplitude predictions are in a reasonable range. Figures 16 shows the prediction historical trends for force locations.

Table 5 shows the reasonable prediction results for different excitation frequencies except for the case of (*i*,*j*)=(13,6). The possible cause can be the sensor location (*i*=13) near the nodal points of modes 2 and 3. Their modal response at such a location can be relatively small and result in bad prediction. Figures 17 shows the prediction historical trends for force locations. As one can see, the force location and amplitude converge to optimal values near to the correct ones except for the case of (*i*,*j*)=(13,6), f_s =70Hz.

Table 6 shows very good prediction of force locations for different sensor locations for $f_s = 14.02\text{Hz} \approx f_1$, and Figure 18 shows the prediction historical trends. The force amplitude prediction errors are near 30% for two cases of (*i*,*j*)=(11,5) and (*i*,*j*)=(13,5). The cause can be the sensor located near the nodal points. From the experiments, we may conclude that the force prediction model can reasonably predict the harmonic force amplitude and location simultaneously, if the sensor is properly mounted away from nodal points of structural mode shapes.

VI. Conclusions

This paper successfully applies the eddy current sensor to detect the beam displacement response due to unknown harmonic force and predicts its force amplitude and location simultaneously. The force prediction model are numerically simulated and experimentally verified to show the feasibility and capability for different force amplitudes, locations and excitation frequencies as well as different sensor locations. With the proper selection of sensor locations away from nodal points of mode shapes, the prediction algorithm can reasonably predict the

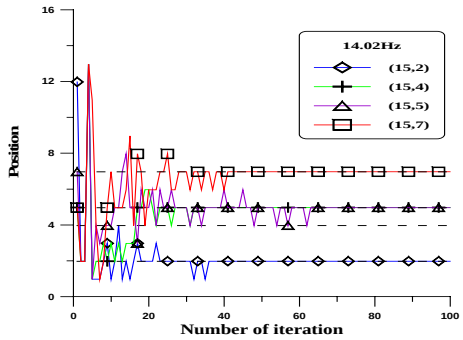

Figure 15. Option (II): prediction results for different force locations, $f_s = 14.02\text{Hz} \approx f_1$

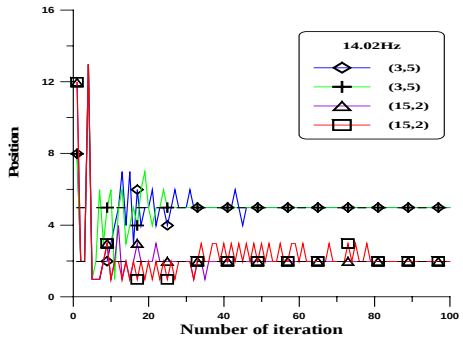

Figure 16. Option (II): prediction results for different force amplitudes, $f_s = 14.02\text{Hz} \approx f_1$

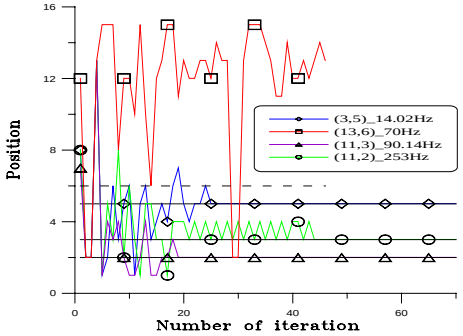

Figure 17. Option (II): prediction results for different excitation frequencies

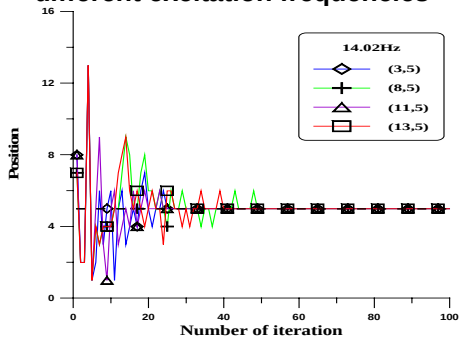

Figure 18. Option (II): prediction results for different sensor locations, $f_s = 14.02\text{Hz} \approx f_1$

Table 3. Option (II): prediction results for different force locations, $f_s = 14.02\text{Hz} \approx f_1$

(i,j)	Actual Force Amplitude (N)	Predicted Force Amplitude (N)	Error (%)	Predicted Force Location
(15,2)	0.476	0.520	9.24	2
(15,4)	0.274	0.213	-22.26	**5**
(15, 5)	0.143	0.154	7.69	5
(15,7)	0.0536	0.0729	36.01	7

Table 4. Option (II): prediction results for different force amplitudes, $f_s = 14.02\text{Hz} \approx f_1$

(i,j)	Actual Force Amplitude (N)	Predicted Force Amplitude (N)	Error (%)	Predicted Force Location
(3,5)	0.179	0.223	24.58	5
(3,5)	0.290	0.305	5.17	5
(15,2)	0.476	0.520	9.24	2
(15,2)	0.533	0.588	10.32	2

Table 5. Option (II): prediction results for different excitation frequencies

(*i*,*j*)	Excitation Frequency (Hz)	Actual Force Amplitude (N)	Predicted Force Amplitude (N)	Error (%)	Predicted Force Location
(3,5)	14.02	0.290	0.305	5.17	5
(13,6)	70	0.385	1.5	289.61	**13**
(11,3)	90.14	0.262	0.196	-25.19	3
(11,2)	253	0.11	0.130	18.18	2

Table 6. Option (II): prediction results for different sensor locations, $f_s = 14.02\text{Hz} \approx f_1$

(i,j)	Actual Force Amplitude (N)	Predicted Force Amplitude (N)	Error (%)	Predicted Force Location
(3,5)	0.290	0.305	5.17	5
(8,5)	0.251	0.223	-11.16	5
(11,5)	0.131	0.167	27.48	5
(13,5)	0.153	0.200	30.72	5

harmonic force amplitudes and locations, simultaneously. The merit of the developed algorithm is that only one location index and force amplitude are considered as design variables and make the optimization problem simple and efficiency to solve. The developed harmonic force prediction methodology can be extended to other engineering structures. In particular, the use of non-contact ECS will be applicable to rotor systems and lead to the prediction of imbalance force effect.

VII. Acknowledgement

The authors gratefully thank the financial support of this work from National Science Council, TAIWAN under the contract number: NSC93-2212-E-020-006.

VIII. Reference

1. Verhoeven, J., 1988, "Excitation Force Identification of Rotating Machines Using Operational Rotor/Stator Amplitude Data and Analytical Synthesized Transfer Functions," *ASME Journal of Vibration, Acoustics, Stress, and Reliability in Design*, Vol. 110, pp. 307-314.
2. Karlsson, S. E. S., 1996, “Identification of External Loads From Measured Harmonic Responses,” *Journal of Sound and Vibration*, Vol. 196, No. 1, pp. 59-74.
3. D’Cruz, J., Crisp, J. D. C., and Ryall, T. G., 1992, “On the Identification of a Harmonic Force on a Viscoelastic Plate from Response Data,” *ASME Journal of Applied Mechanics*, Vol. 59, pp. 722-729.
4. Wang, B. T., 2002, “Prediction of Impact and Harmonic Forces Acting on Arbitrary Structure: Theoretical Formulation," *Mechanical Systems and Signal Processing*, Vol. 16, No. 6, pp. 935-953.
5. Wu, E., Yeh, J. C. and Yen, C. S., 1994, “Impact on Composite Laminated Plates: An inverse Method,” *International Journal of Impact Engineering*, Vol. 15, No. 4, pp. 417-433.
6. Wu, E., Yen, J. C. and Yen, C. S., 1994, “Identification of Impact Forces at Multiple Locations on Laminated Plates,” *AIAA Journal*, Vol. 34, No. 12, pp. 2433-2439.
7. Wang, B. T., and Lin, K. Y., 2004, “Prediction of Harmonic Force Acting on Cantilever Beam,” *Proceedings of the 18th International Modal Analysis Conference*, Dearborn, Michigan, Paper No. 64, Session 3.
8. Wang, B. T., and Chui, T. S., 2003, “Determination of Unknown Impact Force Acting on Simply Supported Beam,” *Mechanical Systems and Signal Processing*, Vol. 17, No. 3, pp. 683-704.
9. Varoto, P. S., and McConnell, K. G., 1997, “Predicting Random Excitation Forces From Acceleration Response Measurements,” *Proceedings of The 15th International Modal Analysis Conference*, pp. 1-6.
10. Liu, D. M., Tsai, C. Z., and Wu, E.,1997, “A New Non-contact Technique to Identify Impact Force of Beam Structure,” *Proceedings of 14th national Conference of the Chinese Society of Mechanical Engineers*, pp. 347-354. (In Chinese)
11. Choi, K., and Chang, F. K., 1996, “Identification of Impact Force and Location Using Distributed Sensors,” *AIAA Journal*, Vol. 34, No. 1, pp. 136-143.
12. Sadler, D. J., and Ahn, C. H., 2001, “On-Chip Eddy Current Sensor for Proximity Sensing and Crack Detection,” *Sensors and Actuators*, Vol. 91, pp. 346-351.
13. Wilde, J., and Lai, Y., 2003, “Design Optimization of an Eddy Current Sensor Using the Finite-Elements Method,” *Microelectronics Reliability*, Vol. 43, pp. 345-349.
14. Yamaguchi, T., Iwai, Y., Inagaki, S., and Ueda, M., 2003, “A Method for Detecting Bearing Wear in a Drain Pump Utilizing an Eddy-Current Displacement Sensor,” *Measurement*, Vol. 33, pp. 205-211.
15. Meirovich, L., 1967, *Analytical Methods in Vibrations*, Macmillan Publishing Co., Inc., New York.
16. Compaq Computer Corporation, 2001, Compaq Visual Fortran Version 6.6, Houston, Texas.
17. Visual Numerics, Inc., 1997, *IMSL Fortran Subroutines for Mathematical Applications,* Vol. 1 and 2, Visual Numerics, Inc.
18. Wang, B. T., Lu, S. H., and Lin, G. Y., “Application of Eddy Current Sensor to the Structural Modal Testing,” *Proceedings of the 25th Conference on Theoretical and Applied Mechanics*, pp. 2171-2182. (In Chinese)